Instantaneous normal mode analysis of the vibrational relaxation of the amide I mode of alanine dipeptide in water

Cite as: J. Chem. Phys. **138**, 205102 (2013); https://doi.org/10.1063/1.4805086
Submitted: 16 January 2013 . Accepted: 01 May 2013 . Published Online: 24 May 2013

Marwa H. Farag, José Zúñiga, Alberto Requena, and Adolfo Bastida

Instantaneous normal mode analysis of the vibrational relaxation of the amide I mode of alanine dipeptide in water

Marwa H. Farag, José Zúñiga, Alberto Requena, and Adolfo Bastida[a)]
Departamento de Química Física, Regional Campus of International Excellence "Campus Mare Nostrum", Universidad de Murcia, 30100 Murcia, Spain

(Received 16 January 2013; accepted 1 May 2013; published online 24 May 2013)

Nonequilibrium Molecular Dynamics (MD) simulations coupled to instantaneous normal modes (INMs) analysis are used to study the vibrational relaxation of the acetyl and amino-end amide I modes of the alanine dipeptide (AlaD) molecule dissolved in water (D_2O). The INMs are assigned in terms of the equilibrium normal modes using the Effective Atomic Min-Cost algorithm as adapted to make use of the outputs of standard MD packages, a method which is well suited for the description of flexible molecules. The relaxation energy curves of both amide I modes show multiexponential decays, in good agreement with the experimental findings. It is found that ~85%–90% of the energy relaxes through intramolecular vibrational redistribution. The main relaxation pathways are also identified. The rate at which energy is transferred into the solvent is similar for the acetyl-end and amino-end amide I modes. The conformational changes occurring during relaxation are investigated, showing that the populations of the alpha and beta region conformers are altered by energy transfer in such a way that it takes 15 ps for the equilibrium conformational populations to be recovered after the initial excitation of the AlaD molecule. © *2013 AIP Publishing LLC*. [http://dx.doi.org/10.1063/1.4805086]

I. INTRODUCTION

The study of the vibrational energy flow in proteins is a fascinating topic due to its deep implication into the connection between structural changes and function of these molecules.[1–4] The most detailed information about intramolecular vibrational redistribution (IVR) comes in this respect from ultrafast time-resolved Infrared/Raman spectroscopy.[5–17] However, the complexity of even the simplest proteins makes the interpretation of these experiments quite difficult, and small peptide molecules are then resorted as models to investigate the peptide backbone dynamics.[18–20] In this context the alanine dipeptide (AlaD) molecule ($CH_3CONHCHCH_3CONHCH_3$, see Figure 1) emerges, which is one of the simplest polypeptides that can be used to explore different conformations in water solution at room temperature.

The conformations of the AlaD molecule,[18,21] namely C5, β, P_{II}, $C7_{eq}$, α_R, α', are defined by the flexible torsion angles ϕ (C-N-C_α-C) and ψ (N-C_α-C-N).[22] High level *ab initio* studies[23,24] of the isolated alanine dipeptide lead to the general conclusion, supported by gas-electron diffraction analysis,[25] that the internally hydrogen bonded conformation $C7_{eq}$ and the extended conformation C5 are the lowest in energy. Structural and thermodynamics characterization of AlaD in water solution by both theoretical methods[18,26–37] and experimental techniques,[38–44] have, however, been unable to date to fully solve the conformational distribution of the molecule in the aqueous environment. Nuclear magnetic resonance (NMR) experiments[38,39,41] favor the P_{II} conformation as the most stable one, in line with some Raman and IR spectroscopic studies,[44] whereas two-dimensional IR spectroscopy[33] and Vibrational Circular Dichroism[43] (VCD) measurements seem to support the P_{II}-like or β conformations in this sense. In contrast, some Raman spectroscopy experiments point out to the predominance of the α_R and $C7_{eq}$ conformations.[40] On the other hand, all the theoretical studies confirm the presence of P_{II}-like or β conformations and some report significant contributions of α_R conformations.[21,27–29,32,34–36] It has been also shown that the relative percentage of the α and β conformers strongly depends on the force field used to simulate the system.[35,36]

From a dynamical point of view, Hochstrasser *et al.*[33] have studied the vibrational relaxation of the amide I modes of the deuterated alanine dipeptide ($CH_3CONDCHCH_3CONDCH_3$, AlaD-d_2) molecule in liquid D_2O using multidimensional infrared spectroscopies. They show that the linear spectra of the AlaD-d_2 molecule is consistent with the picture of the two amide I modes approximately localized at the ends of the peptide. The spectrum in the amide I region is found to comprise two overlapping bands centered at 1629 and 1642 cm^{-1}, which correspond, respectively, to the acetyl-end (CH_3–COND–) and the amino-end (–COND–CH_3) modes. To excite each of the amide I modes selectively, Hochstrasser *et al.*[33] increase the frequency gap by substituting $^{12}C{=}O$ with $^{13}C{=}O$ in the acetyl-end amide I group of the AlaD-d_2 molecule. The frequency of the acetyl-end amide I band of the resulting ^{13}C-AlaD-d_2 molecule is thus redshifted up to 1589 cm^{-1}, while the amino-end one is blueshifted by only 1 cm^{-1}. Interestingly, the vibrational relaxation curves of amide I

a)Electronic mail: bastida@um.es.

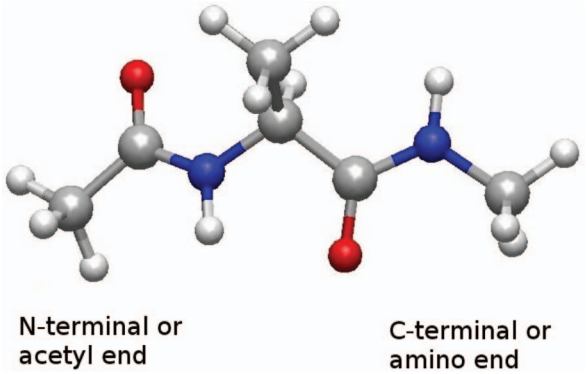

FIG. 1. The alanine dipeptide molecule.

modes show both multiexponential decays, each with different lifetimes and weights, pointing to the existence of different relaxation pathways.

In this paper we conduct nonequilibrium Molecular Dynamics (MD) simulations of the vibrational relaxation of the amide I modes of the AlaD molecule in liquid D_2O. In line with previous works by our group,[45–48] we analyze the results of the MD simulations using the instantaneous normal modes (INMs), which allows us to monitor the time evolution of the energy stored in every vibrational mode and to determine the magnitudes and lifetimes of the different relaxation pathways. Special attention is paid to the evaluation of the conformational changes of the AlaD molecule during the relaxation process. The paper is organized as follows. In Sec. II, we describe the INMs analysis, as adapted to describe flexible molecules, and give the computational details. Sec. III contains the numerical results and discussion including, successively, the choice of the force field used to describe the AlaD molecule, the equilibrium normal modes (ENMs) of the isolated AlaD molecule, the INMs of the AlaD molecule dissolved in water, and the vibrational relaxation of the amide I modes. The conclusions are given in Sec. IV.

II. METHODOLOGY

A. INMs analysis

Our group has recently proposed and implemented[45–48] the use of the INMs analysis to monitor the time evolution of the vibrational energy of a biomolecule in solution after its initial vibrational excitation. The INMs provide a decoupled harmonic description of the vibrational motions of the molecule at any instantaneous configuration, which allows us to evaluate the time-dependent energies and populations of the molecular vibrational modes and, thus, compare them directly with data extracted from time-resolved Infrared/Raman experiments.[49]

To accomplish this task, the INMs have to be continuously identified during the relaxation process as the biomolecule explores different regions of potential energy surface since they are susceptible to substantial changes over time. The identification of the INMs by simple sorting in increasing order of frequencies has been revealed in this sense to be useless[45–47] due to the frequent crossings of the time-dependent frequencies. To amend this problem, we have proposed[45–48] tracking the identity of the INMs by using the ENMs as templates. At each instantaneous snapshot, the INMs are assigned in a one-to-one correspondence with the ENMs by maximizing the overlap between both sets of normal modes, using the so-called Min-Cost algorithm.[45] This methodology, however, presents two drawbacks. The first comes from the fact that the ENMs of the solute molecule are derived from a given body-fixed coordinate set. Application of the Min-Cost algorithm to data extracted from standard MD package, which are based on the use of space-fixed atomic Cartesian coordinates, requires the implementation of the nontrivial transformations between the both body-fixed and space-fixed coordinate sets. This problem becomes particularly difficult to tackle for highly flexible molecules such as polypeptides exhibiting different local minima conformations. The second drawback lies in the overlaps between the ENMs and the INMs, which are evaluated by performing the corresponding dot products between them. This procedure is not well-founded for atoms such as the hydrogens of the $-CH_3$ or $-NH_2$ groups, which can frequently exchange their positions by crossing low or quite flat potential energy barriers, with the consequence that the Cartesian coordinates of these atoms are exchanged during the dynamics, thus modifying the values of the ENMs-INMs overlaps.

In order to facilitate the application of the INMs analysis to the description of flexible molecules using standard MD codes, we have modified the Min-Cost algorithm as follows. First, we evaluate the equilibrium Hessian matrix of the solute molecule in terms of the space-fixed mass-weighted Cartesian $\boldsymbol{q}$ coordinates, K^{E}, whose matrix elements are

$$k_{ij}^{\mathrm{E}} = \left(\frac{\partial^2 V_{\mathrm{intra}}}{\partial q_i \partial q_j}\right)_{\mathrm{E}} \quad i, j = 1, \ldots, 3N_s, \tag{1}$$

where N_s is the number of atoms of the solute molecule, V_{intra} is the solute intramolecular potential energy function, and subscript E indicates that the derivatives are evaluated at the equilibrium configuration of the isolated solute molecule. Diagonalization of the $\boldsymbol{K}^{\mathrm{E}}$ matrix then provides the eigenvector matrix $\boldsymbol{L}^{\mathrm{ENM}}$, which relates the ENMs ($\boldsymbol{Q}^{\mathrm{ENM}}$) with the $\boldsymbol{q}$ coordinates in the form

$$Q_i^{\mathrm{ENM}} = \sum_{j=1}^{3N_s} l_{ji}^{\mathrm{ENM}} q_j \quad i = 1, \ldots, 3N_s. \tag{2}$$

As observed in this expression, the six normal modes associated to the translational and rotational motions of the solute molecule are included in the $\boldsymbol{Q}^{\mathrm{ENM}}$ vector. Next, the instantaneous Hessian matrix of the solute molecule in terms of the $\boldsymbol{q}$ coordinates, $\boldsymbol{K}^{\mathrm{I}}$, whose matrix elements are given by

$$k_{ij}^{\mathrm{I}} = \left(\frac{\partial^2 (V_{\mathrm{intra}} + V_{\mathrm{inter}})}{\partial q_i \partial q_j}\right)_{\mathrm{I}} \quad i, j = 1, \ldots, 3N_s \tag{3}$$

is evaluated at any given time of the dynamics, where, as observed, the intermolecular potential energy that describes the solute-solvent interactions is included. Subscript I stands now for a given instantaneous configuration of the solute and the solvent molecules. The elements of the $\boldsymbol{K}^{\mathrm{I}}$ matrix evolve over time as does the corresponding eigenvector matrix $\boldsymbol{L}^{\mathrm{INM}}$,

which relates the INMs ($\boldsymbol{Q}^{\mathrm{INM}}$) to the $\boldsymbol{q}$ coordinates as follows

$$Q_i^{\mathrm{INM}} = \sum_{j=1}^{3\,N_s} l_{ji}^{\mathrm{INM}}\, q_j \quad i = 1, \ldots, 3\,N_s. \tag{4}$$

In order to quantify the similarity between the ENMs and INMs, we introduce the overlap matrix $\boldsymbol{O}$, whose matrix elements are given by

$$O_{ij} = \sum_{k=1}^{N_s} A_{ki}^{\mathrm{ENM}}\, A_{kj}^{\mathrm{INM}} \quad i, j = 1, \ldots, 3\,N_s \tag{5}$$

with

$$A_{ki}^{\mathrm{ENM}} = \sqrt{\left(l_{3k-2,i}^{\mathrm{ENM}}\right)^2 + \left(l_{3k-1,i}^{\mathrm{ENM}}\right)^2 + \left(l_{3k,i}^{\mathrm{ENM}}\right)^2} \quad k = 1, \ldots, N_s \quad i = 1, \ldots, 3\,N_s \tag{6}$$

and

$$A_{kj}^{\mathrm{INM}} = \sqrt{\left(l_{3k-2,j}^{\mathrm{INM}}\right)^2 + \left(l_{3k-1,j}^{\mathrm{INM}}\right)^2 + \left(l_{3k,j}^{\mathrm{INM}}\right)^2} \quad k = 1, \ldots, N_s \quad j = 1, \ldots, 3\,N_s. \tag{7}$$

The A_{ki}^{ENM} and A_{kj}^{INM} parameters measure the contribution of the mass-weighted space-fixed Cartesian coordinates of atom k to the ith ENM and the jth INM, respectively. Values of the overlaps close to one mean, therefore, that the corresponding ENMs and INMs account for the displacements of the same atoms with similar contributions. The specific values of the three l's elements associated to a given atom change with global or partial rotations of the solute molecule due to variations of the torsional angles. In contrast, the values of the A's parameters remain constant for any internal or global rotation of the molecule because they depend only on the total contribution of all the atoms to a given normal mode, regardless of the molecule orientation. The values of the A's parameters are, moreover, independent of the space-fixed coordinate system used to describe the molecule. The use of the overlap matrix $\boldsymbol{O}$, written in terms of the A's parameters instead of the dot products of the ENMs and INMs used in our previous works,[45–48] allows us to describe flexible molecules properly, and in addition, obviates the use of body-fixed coordinate systems. We should note, however, that the reduction of the modes dimensionality from $3\,N_s$ to N_s may alter the sensibility of the assignment method, since different INMs may have similar atomic contributions. Moreover, the $\boldsymbol{O}$ matrix is not orthonormal so it is necessary to analyze the distribution of its element values. These points are discussed in Sec. III C.

In the INMs assignment method, one has to deal also with the nearly free rotations of some functional groups such as $-CH_3$, $-NH_2$, … which at room temperature can exchange the contributions of the H atoms to the normal modes. These contributions are considered collectively in this work. For instance, for the three hydrogens of a given methyl group with atom numbers k, $k+1$, and $k+2$, we use the single A parameter defined as follows

$$A_{3\mathrm{H},i}^{\mathrm{ENM}} = \sqrt{\sum_{r=k}^{k+2} \left[\left(l_{3r-2,i}^{\mathrm{ENM}}\right)^2 + \left(l_{3r-1,i}^{\mathrm{ENM}}\right)^2 + \left(l_{3r,i}^{\mathrm{ENM}}\right)^2\right]} \tag{8}$$

to account for their contribution to the ith ENM. The upper limit of the sum in Eq. (5) reduces in this case to $N_s - 2$. This procedure is applied systematically to all atoms able to exchange their positions in the corresponding functional groups. The final number of terms of the sum in Eq. (5) is referred to as the number of effective atoms.

As stated above, proper identification of the INMs over time in terms of the ENMs requires establishing a one-to-one correspondence between both sets of normal modes. This can be done by using the Min-Cost algorithm[45] to select those elements of the overlap matrix, one from each row and each pertaining to a different column, which maximize the sum of their values. We, thus, refer to the assignment method described above as the Effective Atomic Min-Cost (EAMC) method. We should emphasize that the EAMC method not only identifies the vibrational INMs of the molecule but also the INMs associated with the translational and rotational motions, since all the modes are included in the definition of the overlap matrix. This poses no complications, however, in the identification of the vibrational INMs since they are assigned to the vibrational ENMs, which are those having eigenvalues of the ENM Hessian matrix different from zero.

The EAMC assignment method of INMs may lead to unphysical assignments when two or more INMs have significant contributions of ENMs which have quite separated frequencies.[45,46] Reiterated crossed assignments of the INMs give place then to critical displacements of their averaged frequencies and to large uncertainties in their vibrational energies. This raises a serious problem in monitoring the vibrational energy stored in a given mode, which can nevertheless be overcome by restricting the application of the Min-Cost algorithm to ranges of frequencies with a $\Delta\omega$ width centered at the ENM frequencies ω_i^e.[46,47] Thus only those INMs whose frequencies lie in the window $(\omega_i^e - \Delta\omega/2, \omega_i^e + \Delta\omega/2)$ are susceptible of being assigned to the jth ENM. In practice, this restriction is implemented by giving arbitrary negative high values to the corresponding overlap matrix elements. Although this restriction in the assignment method of the INMs may somehow erode the efficiency of the method at maximizing the overlaps between the two sets of normal modes,[46,47] the choice of reasonable values of $\Delta\omega$ allows us to avoid unphysical assignments of the INMs with just a small decrease of the average values of the overlaps.

B. Computational details

The behavior of the AlaD molecule in water solution has been studied by carrying out MD simulations using the TINKER package v5.0.[50,51] The solute molecule and 248 water molecules were placed in a cubic box with a length chosen to reproduce the experimental density of the liquid. The simulation time step was $\Delta t = 1$ fs, periodic boundary conditions were applied, a cutoff of 10 Å was used for nonbonded interactions and the Ewald sum method was used for the

TABLE I. Dihedral angles (ϕ/ψ) for the AlaD-d_2 molecule at different conformations.

Force field	C5	β	P_{II}	$C7_{eq}$	α_R	α'
AMBER94	(−146.7,170.8)	(−130.0,130.0)	(−73.3,140.0)	(−73.3,65.7)	(−60.0,−50.0)	(−100.0,−5.0)
OPLSAAL	(−152.0,158.3)	(−130.0,130.0)	(−80.0,140.0)	(−79.3,61.6)	(−69.1,−50.0)	(−100.0,−5.0)
CHARMM22	(−151.4,170.6)	(−120.0,130.0)	(−80.0,140.0)	(−81.4,70.6)	(−78.8,−50.0)	(−100.0,−5.0)

long range interactions. The solvent was always described using the flexible TIP3P model included in the CHARMM22[52] force field and different sets of trajectories were run using the AMBER94,[53] the OPLS-AA/L,[54,55] and the CHARMM22[52] force fields to represent the AlaD molecule. Typically, the systems were equilibrated in a NVT ensemble at $T = 300$ K by coupling to a thermal bath[56] during 800 ps. Then equilibrium NVE simulations were run, exporting data every 50 fs in order to evaluate the dihedral angles distributions and to perform the INMs analysis of the AlaD molecule. The size of the statistical sampling required to reach convergence, especially in the conformational distribution, depends on the particular system considered, and ranged from 20 000 snapshots for the AlaD-d_2(AMBER94)/$D_2O_{(l)}$ system up to 200 000 snapshots for the AlaD-d_2(CHARMM22)/$D_2O_{(l)}$ system.

The relaxation of the amide I modes of the AlaD-d_2 and ^{13}C-AlaD-d_2 molecules dissolved in liquid D_2O was analyzed using independent sets of 400 nonequilibrium simulations. The initial conditions for these trajectories were taken from previous equilibrium NVE simulations. In these runs, an excess energy of one vibrational quantum was deposited at $t = 0$ in the solute molecule by displacing the corresponding amide I INM till its energy reached the proper value. The trajectories were then propagated in the NVE ensemble to avoid any interference of the velocity scaling, during 40 ps with a time step of $\Delta t = 0.5$ fs time step and the data (atomic positions, momenta, forces, and Hessian matrix of the solute) were exported every 50 fs. To obtain reasonable statistics for the dihedral angles distribution of the AlaD-d_2 molecule during the relaxation process, we performed longer simulations up to 60 ps for 2660 trajectories in which only molecular configurations (atomic positions and momenta) were exported at 50 fs time intervals (no forces or Hessian matrices) to keep the data stored within a reasonable size.

III. NUMERICAL RESULTS AND DISCUSSION

A. Choice of the force field

The choice of the MM force field becomes crucial to describe the AlaD molecule dissolved in water properly. We have tested three force fields, AMBER94,[53] OPLS-AA/L,[54,55] and CHARMM22.[52]

We have optimized first the structure of the isolated AlaD-d_2 molecule using the *optimize* program included in the TINKER modeling package version 5.0.[50,51] Thus, we found that conformations $C7_{eq}$ and C5 are the only minima of the isolated molecule for the three force fields, with the $C7_{eq}$ conformer having a lower energy than the C5 conformer, in agreement with previous simulations.[52,53,55] These results are also consistent with those obtained from *ab initio* calculations at different levels of theory.[57–61] The stability of the $C7_{eq}$ conformer is justified[26,28,33,40,61–63] by the intramolecular H-bonding formed between the carbonyl group within the acetyl-end and the NH/ND groups within the amino-end, which produces a seven membered ring geometry. In Table I we give the dihedral angles of the AlaD-d_2 molecule for the different equilibrium conformations provided by the three MM force fields. We note that although the P_{II}, α', α_R, and β conformations are not true minima for the isolated AlaD-d_2 molecule, they become more stable when the molecule is immersed in polar solvents due to the intermolecular H-bonds.

In carrying out the INMs analysis, it is important to consider the ENMs associated to every AlaD-d_2 molecule conformer in order to make a proper choice of them. For this purpose we have optimized the geometry of the isolated AlaD-d_2 molecule by keeping the dihedral angles fixed at the typical values of the P_{II}, α', α_R, and β conformations given in Table I. Partially optimized geometries are thus obtained for every conformer that could be present in solution, which are then used to define the corresponding set of ENMs. Since the dihedral angle intervals for every conformer are not well defined, we have found it useful to group them into two conformational regions: the beta region which includes the C5, $C7_{eq}$, P_{II}, and β conformers, and the alpha region which contains the α_R and α' conformers. The ranges of the dihedrals for these two regions are given in Table II. Consideration of these two conformational regions also allows us to reach convergence in the statistical analysis of the time evolution of the conformer populations during the relaxation using a smaller number of trajectories (see Sec. III D 4).

Let us examine the equilibrium normal modes of the optimized geometries, with particular attention to the amide I normal modes. The inspection of ENMs is guided by the experimental results obtained by Hochstrasser *et al.*[42] in the dynamics of the acetyl and amino-end amide I groups of the AlaD-d_2 molecule dissolved in D_2O, using 2D-IR

TABLE II. Definition of the alpha and beta conformational regions for the CHARMM22 force field.

Alpha				Beta			
ϕ_{min}	ϕ_{max}	ψ_{min}	ψ_{max}	ϕ_{min}	ϕ_{max}	ψ_{min}	ψ_{max}
−180	0	−150	30	−180	0	−180	−150
				−180	0	30	180
				150	180	−180	−150
				150	180	30	180

TABLE III. Atomic displacement contributions of the C and O atoms of the amino and acetyl-end carbonyl groups (in %) to the amide I ENMs for different conformations of the isolated AlaD-d_2 molecule, obtained using the AMBER94, OPLS-AA/L, and CHARMM22 force fields.

Force field	ENM	Carbonyl group	C5	β	P_{II}	$C7_{eq}$	α_R	α'
AMBER94	47th	Amino-end	41.7	37.6	26.0	31.9	26.6	31.4
		Acetyl-end	38.2	39.8	50.0	42.0	50.0	47.7
	48th	Amino-end	30.0	30.6	41.6	37.7	46.1	39.6
		Acetyl-end	30.0	28.0	23.8	29.6	23.5	23.7
OPLS-AA/L	47th	Amino-end	42.1	42.6	28.6	23.3	39.9	25.4
		Acetyl-end	37.7	36.5	49.9	54.2	38.6	52.0
	48th	Amino-end	34.8	33.8	46.0	52.4	38.1	50.9
		Acetyl-end	31.5	34.2	24.8	20.0	35.8	20.8
CHARMM22	47th	Amino-end	80.7	84.5	87.0	73.0	0.1	0.4
		Acetyl-end	0.7	0.2	0.2	18.2	91.0	88.0
	48th	Amino-end	0.7	0.2	0.2	16.1	80.2	73.0
		Acetyl-end	85.0	90.0	89.8	74.5	0.1	0.4

TABLE IV. Frequencies (in cm^{-1}) of the amide I modes of the isolated AlaD-d_2 molecule.

Force field	ENM	C5	β	P_{II}	$C7_{eq}$	α_R	α'
AMBER94	47th	1684.5	1685.7	1682.4	1682.0	1685.3	1680.2
	48th	1705.8	1704.9	1699.8	1702.7	1703.0	1712.9
OPLS-AA/L	47th	1678.0	1678.8	1673.8	1672.3	1674.4	1674.4
	48th	1688.9	1685.2	1686.2	1693.8	1687.0	1695.4
CHARMM22	Amino-end	1673.5	1672.7	1670.4	1673.6	1689.6	1693.8
	Acetyl-end	1678.9	1679.0	1678.4	1680.0	1678.6	1677.9

Experiments	Frequency
Ar matrix[a]	1674, 1685, 1698-1701
Ar matrix[b]	1680, 1688, 1704
Kr matrix[b]	1678, 1680, 1702

[a]Reference 69.
[b]Reference 70. Data for the AlaD molecule.

spectroscopy. Hochstrasser *et al.*[42] conclude that the two amide I modes are approximately localized in the carbonyl groups. To test the three MM force fields we give, in Table III, the atomic displacement contributions of the C and O atoms of the amino and acetyl-end carbonyl groups to the two amide I modes, which are the 47th and 48th ENMs in the frequency ordering that excludes in the numbering the normal modes corresponding to the translational and rotational motions of the molecule. As observed in Table III, the sum of the contributions of the carbonyl groups to the amide I ENMs ranges from 60% to 91%, in agreement with the accepted association of the amide I bands to the motions of the C=O groups.[64–66] The amide I ENMs of the AMBER94 and OPLS-AA/L force fields have important contributions from both carbonyl groups. In contrast, the amide I ENMs obtained using the CHARMM22 force field involve the motion of, practically, only one CO group, with the exception of the $C7_{eq}$ conformer, which has a negligible contribution in water solution, as previously discussed.

The fact that two or more modes might be involved in the displacement of the same group of atoms has important consequences in the IVR processes. As Kidera *et al.*[67,68] have shown, the overlap between ENMs correlates with their couplings, and subsequently with the rate of energy transfer among the modes. Our results indicate that the CHARMM22 force field localizes the amide I modes over one carbonyl group of the AlaD-d_2 molecule, in agreement with experiments,[42] whereas in the AMBER94 and OPLS-AA/L force fields the amide I modes are delocalized.

B. Equilibrium normal mode frequencies

In Table IV we give the amide I frequencies provided by the three MM force fields for the different AlaD-d_2 conformers. As observed, the frequency gap between the two amide I modes lies in the 10–20 cm^{-1} range in all cases. For the AMBER94 and OPLS-AA/L force fields, the delocalization of the amide I ENMs over the two carbonyl groups makes it impossible to track their identity through the different conformations. In contrast, since the CHARMM22 force field provides highly localized amide I modes, we can label them as amino and acetyl-end amide I modes for the different conformations as indicated in Table IV. Interestingly, the frequency order of the two amide I groups depends on the conformation. The frequency of the amino-end amide I mode is in particular lower than the frequency of the acetyl-end one for the C5, β, P_{II}, and $C7_{eq}$ conformers, and higher for the α_R and α' conformers. In Table IV we include also the experimental frequencies of the amide I modes of the AlaD-d_2 molecule in argon matrix,[69] since there are no direct measurements of them in vacuum to our knowledge, and the experimental frequencies of these modes for the AlaD molecule in Ar and Kr matrices.[70] The amide I frequencies vary only slightly upon deuteration since the contribution of the H/D atoms of the NH/ND groups to the amide I ENMs is small. The amide I IR bands contain such a bunch of peaks that it is quite difficult to make a one-to-one assignment. It is accepted, however, that the higher frequency corresponds to the amino-end amide I mode,[70] as given by the α_R and α' conformers of the CHARMM22 force field. The agreement between the calculated amide I ENM frequencies obtained for the three MM force fields and the experimental values is found to be overall satisfactory.

The above considerations on the localization and the frequency values of the amide I modes indicate that the CHARMM22 MM force field is the most appropriate to study the vibrational relaxation of the AlaD-d_2 system. In Table S.M.I of the supplementary material[71] we give the ENM frequencies of the different conformations of isolated AlaD-d_2 molecule calculated using the CHARMM22 force field. As observed, there are some differences among the frequencies of the conformers which, nevertheless, become minor as the frequency increases. The higher frequency vibrational modes are, therefore, less affected by the molecular conformation, as expected, since these modes correspond mostly to highly localized bending and stretching vibrations which tend to be largely unaffected by the wide atomic displacements involved in the conformational changes. In contrast, the lower frequency modes are much more delocalized,[67,68] involving simultaneous and wide motions of many atoms, with the

interatomic interactions being then much more prone to vary from one conformer to another.

C. Instantaneous normal modes

The next issue that we address is the analysis of the equilibrium vibrational properties of the AlaD-d_2/$D_2O_{(l)}$ system, as extracted from the CHARMM22 force field. This analysis is important in order to assess the ability of the EAMC algorithm to assign the INMs of the AlaD-d_2 molecule during the simulations. In Table S.M.II of the supplementary material[71] we give the time averaged INM frequencies obtained using the EAMC method with a frequency window of 400 cm^{-1} width. The ENMs used as templates correspond to the different conformations included in Table I. The time averaged frequencies in Table S.M.II[71] are ordered according to their ENM assignments. Accordingly, the *i*th INM of a given conformation includes all the INMs contributions from different snapshots of the system which are assigned to the *i*th ENM using the ENMs of that conformer as templates. The resulting INM frequencies do not then remain ordered by increasing values, as the original ENMs are, and comparison of the frequencies within the same row of Table S.M.II[71] is not always appropriate, since the *i*th ENMs of the different conformers can be quite different. This is clearly illustrated by the 47th and 48th ENMs which, as already discussed, correspond, respectively, to the amino and acetyl-end amide I modes of the beta region conformers, whereas their assignments are reversed for the alpha region conformers. We have to compare then the frequencies of the 47th INMs for the beta conformers with the frequencies of the 48th INMs for the alpha conformers, which all have similar values of around 1685.4 cm^{-1}. The data included in Tables III and IV indicate that the 47th INM corresponds to the amino-end amide I mode. Similarly, the 48th INMs of the beta conformers should be compared with the 47th INMs of the alpha conformers. The frequencies of these modes are again very similar, with values around 1683.8 cm^{-1}, and this mode corresponds now to the acetyl-end amide I mode.

The 1683.8 and 1685.4 cm^{-1} INM frequencies obtained for the acetyl and amino-end amide I groups are both some tens of cm^{-1} higher than the 1629 and 1642 cm^{-1} values observed experimentally.[42] Also the difference between the calculated amide I INM frequencies is smaller than the difference between the experimental frequencies, which is due to the frequency order inversion of these modes when the conformation of the molecule goes from the alpha to the beta region, or vice versa. As we will show below, the AlaD-d_2 molecule in D_2O solution widely explores the two conformational regions explaining why the frequency split of these INMs becomes rather small.

In Figure 2 we show the $\boldsymbol{O}$ overlap matrix obtained using the EAMC method with a frequency window of 400 cm^{-1} width, using the ENMs corresponding to the C5 conformer as templates. As observed, the diagonal overlaps are, in general, significantly larger than the off-diagonal overlaps. There are, however, some groups of INMs that do not follow this pattern. These groups of INMs appear as dark rectangles along the diagonal in Figure 2 and, as a consequence, they cannot be identified unambiguously with a single ENM due to recurrent crossed assignments during the simulations. These INMs are gathered according to their nearly degenerated time-averaged vibrational frequencies, as shown in Table V, resulting in the groups 27th–32nd, 35th–42nd, 52nd–56th, and 57th–60th INMs which are mainly formed by rocking methyl, bending methyl, CH stretches, and stretching methyl ENMs, respectively. These groups of mixed INMs have been previously observed[45,46] when the INMs are assigned in terms of the ENMs using the overlaps evaluated through direct dot products between both sets of modes. This behavior is a consequence of the time evolution of the definition of the INMs during the dynamics due to the motion of the solute and solvent molecules. We also observe in Figure 2 some large off-diagonal overlaps far away from the matrix diagonal. However, these overlaps are filtered during the assignment process since they correspond to coupling between ENMs and INMs which frequency gap is larger than the frequency window width. Overall, the average values of the diagonal and off-diagonal overlaps are 0.92 ± 0.07 and 0.48 ± 0.24. The notorious difference between these values shows that the INMs can be reasonably assigned through the overlaps defined in terms of atomic contributions, despite the decrease of the normal modes dimensionality. Moreover, these values remain nearly the same when the ENMs corresponding to the other conformations of the solute are used as templates. This is a consequence of the similarity of the different sets of ENMs. In fact, the average values of the diagonal overlaps between them as obtained using the EAMC method are around 0.95 ± 0.05 in all the cases. The INM analysis based on the application of the EAMC method reveals as an efficient method to identify the INMs, with the efficiency of the assignments not depending on the choice of the ENMs used as templates. This finding is very encouraging in order to extend the INM analysis to polypeptides and proteins, where the number of conformers becomes huge, making it impossible to perform

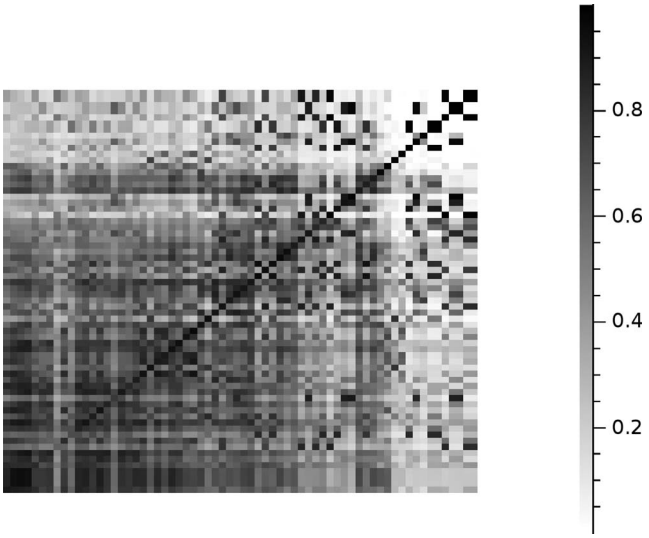

FIG. 2. Overlap matrix between ENMs and INMs obtained as defined in Eq. (5) using the EAMC method with a frequency window of $\Delta\omega = 400$ cm^{-1} width and the ENMs corresponding to the C5 conformer as templates.

TABLE V. Time averaged vibrational frequencies and standard deviations (in cm^{-1}) of the INMs of the AlaD-d_2 and ^{13}C-AlaD-d_2 molecules in liquid D_2O obtained using the EAMC method with a frequency window of $\Delta\omega = 400\ cm^{-1}$ width. The ENMs used as templates are those of the C5 conformers.

INM	AlaD-d_2	^{13}C-AlaD-d_2	INM	AlaD-d_2	^{13}C-AlaD-d_2
1	43.7 ± 110.3	42.3 ± 110.0	31	1074.8 ± 47.7	1058.1 ± 71.2
2	− 141.7 ± 236.9	− 144.5 ± 238.7	32	1075.9 ± 70.3	1097.3 ± 68.4
3	70.6 ± 133.6	70.8 ± 134.8	33	1178.3 ± 36.6	1172.1 ± 40.7
4	− 15.3 ± 252.1	− 15.8 ± 252.6	34	1304.9 ± 45.4	1301.6 ± 47.8
5	159.6 ± 111.4	159.0 ± 112.6	35	1395.3 ± 42.7	1381.6 ± 47.0
6	219.8 ± 95.9	219.1 ± 94.9	36	1406.9 ± 80.7	1407.3 ± 81.4
7	182.3 ± 109.1	184.0 ± 109.0	37	1422.9 ± 86.6	1419.7 ± 75.3
8	226.5 ± 81.6	226.6 ± 83.0	38	1422.1 ± 74.5	1416.9 ± 69.9
9	295.2 ± 100.6	294.3 ± 102.5	39	1419.2 ± 49.6	1416.9 ± 69.6
10	171.4 ± 277.6	168.1 ± 279.5	40	1410.7 ± 61.8	1417.5 ± 60.7
11	308.0 ± 85.1	307.1 ± 85.7	41	1427.3 ± 51.0	1429.4 ± 51.9
12	355.8 ± 71.9	356.3 ± 73.7	42	1430.7 ± 60.9	1432.7 ± 74.2
13	418.3 ± 73.7	419.3 ± 73.5	43	1448.2 ± 62.4	1459.4 ± 53.9
14	519.2 ± 59.2	533.5 ± 61.4	44	1463.5 ± 50.7	1449.6 ± 63.0
15	575.2 ± 133.5	576.7 ± 128.9	45	1583.4 ± 59.0	1558.5 ± 74.2
16	557.7 ± 64.4	563.7 ± 84.5	46	1549.4 ± 67.8	1559.1 ± 72.9
17	569.2 ± 94.3	539.2 ± 71.4	47	1684.9 ± 11.0	1638.3 ± 3.9
18	620.1 ± 48.5	616.7 ± 45.0	48	1683.8 ± 4.2	1685.7 ± 11.3
19	746.0 ± 61.2	745.6 ± 70.8	49	2444.6 ± 3.9	2444.7 ± 3.8
20	771.3 ± 58.9	768.5 ± 48.8	50	2442.9 ± 4.0	2442.6 ± 4.0
21	786.2 ± 53.4	785.5 ± 53.8	51	2858.4 ± 6.7	2858.3 ± 6.7
22	844.8 ± 36.3	843.9 ± 37.5	52	2909.5 ± 17.0	2909.5 ± 19.4
23	854.4 ± 63.9	854.8 ± 63.7	53	2911.0 ± 11.4	2911.1 ± 11.5
24	922.1 ± 71.0	921.7 ± 70.2	54	2925.0 ± 11.1	2925.2 ± 11.2
25	973.9 ± 69.0	983.2 ± 73.5	55	2915.4 ± 15.5	2915.1 ± 15.5
26	997.4 ± 68.5	998.3 ± 72.5	56	2923.3 ± 8.4	2923.1 ± 8.5
27	1004.9 ± 77.9	1005.7 ± 80.4	57	2965.5 ± 18.5	2965.4 ± 18.7
28	1064.2 ± 63.7	1071.9 ± 56.3	58	2966.0 ± 12.3	2966.0 ± 12.6
29	1040.3 ± 59.3	1029.3 ± 61.3	59	2976.7 ± 20.6	2976.3 ± 22.7
30	1080.0 ± 71.5	1050.8 ± 106.0	60	2986.9 ± 27.8	2987.0 ± 35.1

an individual analysis of every set of ENMs. In the rest of the paper, we use the ENMs corresponding to the C5 conformer as templates.

From an experimental point of view, the study of the vibrational relaxation of the acetyl and amino-end amide I modes of the AlaD-d_2 molecule gets complicated due to the overlap between the bands of the two modes.[42] Hochstrasser *et al.*[42] managed to excite each amide I mode selectively using ^{13}C isotopic substitution of the carbon atom of the carbonyl group in the acetyl-end of the AlaD-d_2 molecule. This results in a 40 cm^{-1} redshift of the acetyl-end band of the ^{13}C-AlaD-d_2 molecule, up to 1589 cm^{-1}, and an only 1 cm^{-1} blueshift of the amino-end band, up to 1643 cm^{-1}, with a frequency gap, therefore, of 54 cm^{-1} between the two bands of the ^{13}C-AlaD-d_2 molecule which enables selective excitation. In Table V we give the averaged INMs frequencies calculated for the AlaD-d_2 and ^{13}C-AlaD-d_2 molecules along with the corresponding standard deviations which measure the magnitude of the frequency fluctuations during the dynamics due to the time evolution of the intra- and intermolecular interactions. As observed, the ^{13}C isotopic substitution results in a smaller value of the frequency of the acetyl-end amide I mode than that of the amino-end mode for the ^{13}C-AlaD-d_2 molecule, with the 47th and 48th INMs corresponding to the acetyl and amino-end amide I modes, respectively. Comparison of the calculated amide I frequencies reveals in turn that the frequency of the acetyl-end amide I mode is redshifted by 46.6 cm^{-1} up to 1638.3 cm^{-1}, while the frequency of the amino-end amide I band is hardly affected by a small 1.9 cm^{-1} redshift taking it up to 1685.7 cm^{-1}. The theoretical frequency gap between both amide I modes is 47.4 cm^{-1}. Although our MD simulations overestimate the frequencies of the two amide I modes by 40 cm^{-1}, and underestimate the frequency gap by 7 cm^{-1}, we think that these deviations are small enough to consider our MD simulations reliable.

D. Vibrational relaxation of the amide I modes

Let us consider now the vibrational relaxation of the amide I modes of the ^{13}C-AlaD-d_2 molecule in liquid D_2O, as simulated by running two independent sets of 400 trajectories, each corresponding to initial excitation of every amide I mode.

1. Amide I modes relaxation lifetimes

In Figures 3(a) and 3(b) we show the time evolution extracted from the simulations of the vibrational energy of the

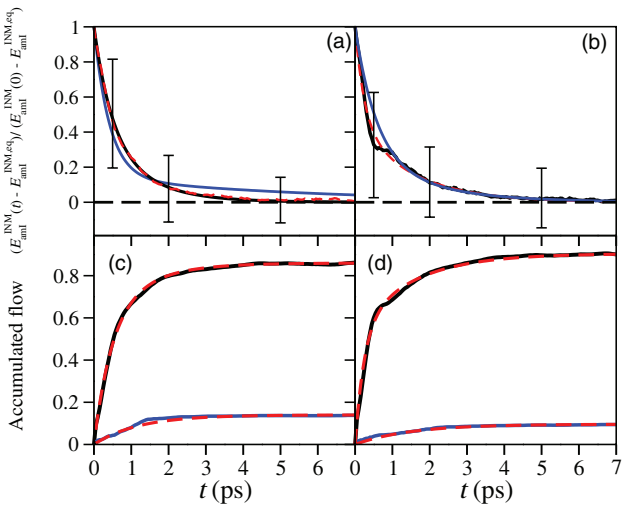

FIG. 3. Time evolution of the normalized vibrational energy of the (a) acetyl and (b) amino-end amide I modes of the ^{13}C-AlaD-d_2 molecule in liquid D_2O, with respect to their equilibrium values, at 300 K (black lines), including in addition the corresponding fits to Eq. (9) (red dashed lines) and to the experimental data (blue lines), and time evolution of the normalized accumulated energy that flows from the (c) acetyl and (d) amino-end amide I modes into the remaining INMs of the ^{13}C-AlaD-d_2 molecule through IVR processes (black lines) and into the solvent (blue lines), along with their fits (red dashed lines) to Eqs. (10) and (11), respectively. Error bars are the standard deviations of the energy curves corresponding to the 400 trajectories statistics.

acetyl and amino-end amide I modes, respectively, after their initial excitation. The relaxation curves are fitted to the following biexponential function

$$\frac{E_{amI}^{vib}(t) - E_{amI}^{vib,eq}}{E_{amI}^{vib}(0) - E_{amI}^{vib,eq}} = \sum_{i=1}^{2} c_{rel,i} e^{-t/\tau_{rel,i}}, \qquad (9)$$

where $E_{amI}^{vib}(t)$, $E_{amI}^{vib}(0)$, and $E_{amI}^{vib,eq}$ are the time-dependent, initial, and equilibrium amide I vibrational energies, respectively, $c_{rel,i}$ are the amplitudes, with $c_{rel,1} + c_{rel,2} = 1$, and $\tau_{rel,i}$ are the relaxation lifetimes. The fit parameters are given in Table VI. We use then the Statistical Minimum Flow (SMF) method[72] to investigate which amounts of the energy released by the amide I modes are channeled through IVR processes or through intermolecular transfer into the solvent. Accordingly, in Figures 3(c) and 3(d) we show the time evolution of the accumulated energy that flows from the acetyl and amino-end amide I modes to the bath (f_{bath}^{ac}) and to the rest of the INMs of the molecule (f_{IVR}^{ac}), respectively. The resulting energy flow curves are now well reproduced by the functions

$$\frac{f_{IVR}^{ac}(t)}{E_{amI}^{vib}(0) - E_{amI}^{vib,eq}} = \sum_{i=1}^{2} c_i^{IVR}(1 - e^{-t/\tau_i^{IVR}}), \qquad (10)$$

$$\frac{f_{bath}^{ac}(t)}{E_{amI}^{vib}(0) - E_{amI}^{vib,eq}} = c^{bath}(1 - e^{-t/\tau^{bath}}), \qquad (11)$$

where c_i are the amplitudes, with $\sum_{i=1}^{2} c_i^{IVR} + c^{bath} = 1$, and τ_i are the lifetimes. The values obtained for these parameters are also included in Table VI.

Comparison of the lifetimes and weights derived from the kinetic analysis with those obtained using the SMF method indicates that the shorter relaxation time of the amide I mode corresponds to IVR accounting for 60.0% (acetyl-end) and 53.8% (amino-end) of the energy released, while the longer relaxation time characterizes both a secondary IVR process with 26.0% (acetyl-end) and 36.6% (amino-end) weights and the energy flow into the solvent that accounts for only 14.0% (acetyl-end) and 9.6% (amino-end) of the energy released.

In order to compare the MD-INM results with the experimental findings, we include in Figures 3(a) and 3(b) the fits to the measured data,[42] whose parameters are reproduced in Table VI. As observed, during the first 2 ps relaxation of the acetyl amide I mode extracted from the simulations becomes slower than that observed and relaxation of the amino-end amide I mode goes faster than that observed. In general, the agreement between theory and experiment is acceptable, bearing in mind that our results are based on standard MM force fields and that the MD simulations are carried out with no additional adjustable parameters or corrections.

TABLE VI. Vibrational relaxation times (in ps) and amplitudes of the acetyl and amino-end amide I modes of the ^{13}C-AlaD-d_2 molecule in liquid D_2O.

	Amide I	$\tau_{rel,1}$ ($c_{rel,1}$)	$\tau_{rel,2}$ ($c_{rel,2}$)	
Kinetic[a]	Acetyl-end	0.48 (0.600)	1.20 (0.400)	
	Amino-end	0.24 (0.538)	1.49 (0.462)	
Expt.[a,b]	Acetyl-end	0.42 (0.858)	5.70 (0.142)	
	Amino-end	0.58 (0.735)	1.86 (0.265)	
		τ_1^{IVR} (c_1^{IVR})	τ_2^{IVR} (c_2^{IVR})	τ^{bath} (c^{bath})
SMF[c]	Acetyl-end	0.48 (0.600)	1.20 (0.260)	1.20 (0.140)
	Amino-end	0.24 (0.538)	1.49 (0.366)	1.49 (0.096)

[a]Fits to Eq. (9).
[b]Reference 42.
[c]Fits to Eqs. (10) and (11).

2. IVR pathways

Let us consider next the IVR relaxation pathways of the amide I modes. As discussed above, 60.0% of the energy released by the acetyl-end amide I mode is channeled into the molecule through IVR with a lifetime of 0.48 ps. We have located up to 25 different INMs excited in that time scale. These INMs are listed in Table VII, which also includes the parameters obtained by fitting the evolved vibrational energy curves (see Figures S.M.1 and S.M.2 of the supplementary material[71]) to the function

$$E_i^{INM}(t) - E_{i,eq}^{INM} = A\,(e^{-t/\tau_{rel}} - e^{-t/\tau_{exc}}) + B, \qquad (12)$$

where τ_{rel} and τ_{exc} are the relaxation and excitation lifetimes, respectively, A is a parameter related to the maximum of the curve, and B accounts for small deviations of the curve from the equilibrium value at long times due to statistical noise. Some groups of INMs could not be resolved individually, as occurred in our previous studies on the *N*-methylacetamide molecule,[45–48] and they were grouped as acetyl and amino-end CH_3 bending modes and as $C_\beta H_3$ bending modes (see Table VII). The high number of INMs that participate in the relaxation of the amide I modes arises from the multiple

TABLE VII. Parameter values obtained from the fits to Eq. (12) of the vibrational INM energy curves of the ^{13}C-AlaD-d_2 molecule in liquid D_2O after initial excitation of the acetyl and amino-end amide I modes. The relaxation and excitation times are in ps and the values of the A and B parameters in cm^{-1}.

Acetyl-end					Amino-end				
INM	τ_{exc}	τ_{rel}	A	B	INM	τ_{exc}	τ_{rel}	A	B
14th	0.48	4.27	37.9	− 1.9	15th	0.24	2.73	31.9	7.7
15th	0.48	3.79	24.7	5.0	16th	0.24	3.24	22.0	11.1
16th	0.48	1.02	191.0	10.9	20th	0.24	5.23	60.5	3.9
17th	0.48	3.62	48.0	7.0	21st	0.24	4.12	38.5	8.6
18th	0.48	4.5	40.3	2.5	22nd	0.24	1.54	464.6	11.6
20th	0.48	7.10	37.0	7.0	23rd	0.24	4.93	70.3	8.8
24th	0.48	10.6	36.3	7.7	24th	0.24	5.12	61.7	10.8
25th	0.48	3.20	111.5	15.1	27th	0.24	10.3	37.2	4.9
26th	0.48	10.6	45.0	2.8	28th	0.24	6.45	43.2	1.7
28th	0.48	10.6	30.1	1.8	29th	0.24	12.3	24.3	2.7
29th	0.48	4.52	62.9	4.3	34th	0.24	7.25	44.9	3.3
30th	0.48	1.41	290.9	4.1	35th	0.24	10.7	32.6	− 1.2
31st	0.48	10.6	22.0	6.3	43rd	0.24	13.2	30.1	− 3.1
33rd	0.48	10.6	30.8	1.4	45th	0.24	5.09	30.4	10.3
34th	0.48	10.6	26.9	4.0	46th	0.24	6.22	40.3	2.7
35th	0.48	10.6	23.5	4.0					
43rd	0.48	10.6	20.8	1.7	30th	1.49	5.95	43.2	1.3
45th	0.48	10.6	21.4	11.1	31st	1.49	4.29	75.4	6.2
46th	0.48	10.6	19.4	5.7	32nd	1.49	3.73	86.9	4.5
					33rd	1.49	10.5	52.4	− 1.9
CH bending[a]	1.20	10.6	104.8	3.9	CH bending[a]	1.49	12.5	86.7	− 0.5
$C_\beta H$ bending[b]	1.20	10.6	78.9	9.5	CH bending[c]	1.49	8.42	74.7	− 9.5
					$C_\beta H$ bending[b]	1.49	13.2	94.0	4.9
27th	1.40	5.55	58.1	8.2					
49th–60th	1.65	10.6	360.2	21.2	25th	1.60	7.81	44.1	13.1
					26th	1.60	6.36	55.8	6.3
					49th–60th	1.90	13.2	300.1	18.1

[a]Acetyl-end CH_3 bending composed by the 36th, 39th, and 40th INMs.
[b]$C_\beta H_3$ bending composed by the 37th, 42nd, and 44th INMs.
[c]Amino-end CH_3 bending composed by the 38th and 41st INMs.

combinations of INM frequencies that satisfy the resonance condition within the standard deviations of the frequencies of the modes involved (see Table V). In particular, the frequency sums of different combinations of the 14th–20th INMs and the 24th–33rd INMs give values quite close to the acetyl-end amide I mode frequency. Interestingly, one of the best matches is that corresponding to the 16th (twisting of the N-D groups mode) and 30th (rocking (CH_3)N mode) INMs, which are two of the INMs that become more excited during the relaxation process (see Figure S.M.1 of the supplementary material[71]). The second and slower IVR relaxation channel of the acetyl-end amide I mode accounts for 26.0% of the energy and has a lifetime of 1.20 ps. The INMs which are more excited in that time scale are acetyl-end CH_3 and $C_\beta H_3$ bending modes (see Table VII). For the 34th–46th (bending methyl mode) INMs, fulfillment of the resonance condition requires the participation of low frequency modes in the 100–300 cm^{-1} range. The frequencies of these modes appreciably overlap, in turn, with the librational band frequencies of the D_2O solvent,[73] with the consequence that they store small amounts of energy that cannot be quantified in our analysis.

As far as the relaxation of the amino-end amide I mode is concerned, the kinetic and SMF analyses also reveal the existence of two different IVR channels (see Table VI). The faster one has a lifetime of 0.24 ps, accounts for 53.8% of the energy transferred, and involves the participation of 15 INMs whose energy curves also fit well to Eq. (12). The fit parameters are given in Table VII and the energy curves are shown in Figures S.M.3 and S.M.4 of the supplementary material.[71] In this case, the energy flow can be unraveled using again the frequency resonant condition. Either the sum of one frequency the 15th–16th INMs and one frequency of the 27th–29th INMs, or the sum of two frequencies of the 20th–24th INMs, provides values which match well with the amino-end amide I frequency, while the 34th, 35th, 43rd, 45th, and 46th INMs require the participation of low frequency modes that fulfill the resonance condition. Note here the special case of the 22nd INM, which nicely couples to the initially excited mode through a 2:1 Fermi resonance ($2\times843.9 = 1687.6$ cm^{-1}), explaining why this INM receives the largest amount of energy, as shown in Figure S.M.3 of the supplementary material.[71] The second IVR channel for relaxation of the amino-end amide I mode is slower, with a lifetime 1.49 ps, and quantitatively less important since it accounts for 46.2% of the transferred energy. The energy is in this case more evenly distributed among the 30th to the 33rd INMs and the

acetyl-end CH_3, amino-end CH_3, and $C_\beta H_3$ bending modes. The corresponding relaxation energy curves are shown in Figure S.M.5 of the supplementary material[71] and the fitting parameters to Eq. (12) are given in Table VII.

Let us focus our attention now on the secondary IVR processes. In the relaxation of the acetyl-end amide I mode, the 27th INM is the one which receives most energy (see Figure S.M.6 of the supplementary material[71]). The fit parameters to Eq. (12) are included in Table VII and reveal that these INMs become excited after 1.40 ps. Although multiple combinations of previously excited INMs may induce the excitation of the 27th INM mode, we think that the 30th INM is the most likely candidate. Our guess is supported by the fact that the 30th INM receives a significant amount of energy from the initially excited acetyl-end amide I mode (see Figure S.M.1 of the supplementary material[71]), that its frequency is quite close to the frequency of the 27th mode, and that its relaxation time is much shorter than those of the other INMs with similar frequencies (see Table VII). The same arguments explain why excitation of the 25th and 26th INMs (see Figure S.M.7 of the supplementary material[71]), which are the most involved in the secondary IVR processes that follow relaxation of the amino-end amide I mode, presumably occurs through energy flow from the 22nd INM.

As observed in Figure S.M.8,[71] there is some energy flow in our simulations to the 49th–60th (symmetric and asymmetric stretching CH_3 groups modes) INMs, whose frequencies are higher than those of the amide I modes. This unphysical energy transfer from low to high frequency modes is a well-known drawback of classical simulations.[45,46,67,68,72,74,75] In the acetyl case, the high frequency modes are excited at 1.65 ps, so they probably receive the energy from modes previously excited by the amide I mode which have shorter relaxation times, such as the 16th and 30th INMs. In the amino-end case, the excitation time of the high frequency modes is 1.90 ps, and the energy may come directly from the initially excited mode or, more likely, from some bending modes through an efficient 2:1 Fermi resonance, as found in previous studies on the deuterated N-methylacetamide (NMAD) molecule.[45,46,72] The amount of energy stored in these high frequency modes is, nevertheless, just ∼12% of the amide I vibrational quantum and its effect on the whole IVR process is therefore minor. Interestingly, this percentage of energy is smaller than the 18% found in the relaxation of the NMAD amide I mode in D_2O solution.[72] This difference could be explained by the higher density of vibrational states in the ^{13}C-AlaD-d_2 molecule compared with that of NMAD, which presumably favors the transfer of energy to lower frequency modes.

3. Energy transfer into the solvent

In Figure 4, we plot the time evolution of the normalized vibrational energy of the ^{13}C-AlaD-d_2 molecule in liquid D_2O after excitation of both the acetyl and the amino-end amide I modes. The two curves fit well to the biexponential function

$$\frac{E^{\rm vib}_{\rm AlaD}(t) - E^{\rm vib,eq}_{\rm AlaD}}{E^{\rm vib}_{\rm AlaD}(0) - E^{\rm vib,eq}_{\rm AlaD}} = c_{\rm rel,1}\, e^{-t/\tau_{\rm rel,1}} + c_{\rm rel,2}\, e^{-t/\tau_{\rm rel,2}} \qquad (13)$$

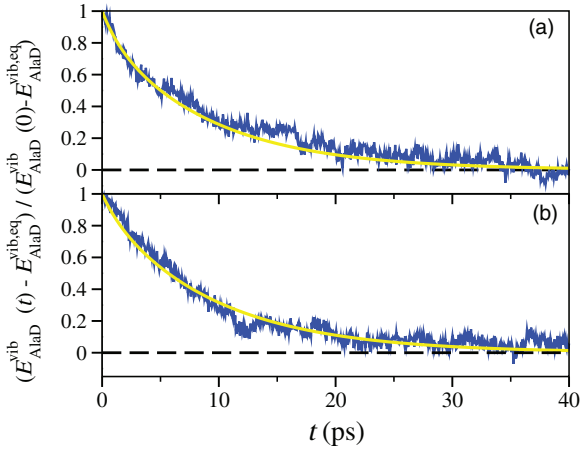

FIG. 4. Time evolution of the normalized vibrational energy of the ^{13}C-AlaD-d_2 molecule in liquid D_2O after initial excitation of the (a) acetyl and (b) amino-end amide I modes (blue lines) and the corresponding fits to Eq. (13) (yellow line).

with the parameter values $\tau^{\rm acend}_{\rm rel,1} = 1.20$ ps (14.0%) and $\tau^{\rm acend}_{\rm rel,2} = 10.6$ ps (86.0%) for the relaxation of the acetyl-end amide I mode, and $\tau^{\rm amend}_{\rm rel,1} = 1.49$ ps (9.6%) and $\tau^{\rm amend}_{\rm rel,2} = 9.51$ ps (90.4%) for the relaxation of the amino-end amide I mode. In both cases the shortest relaxation times and their weights account for the direct energy transfer from the amide I modes to the solvent (see Table VI), whereas the longest relaxation times are to be interpreted as average time values accounting for the different energy transfer processes from the remaining INMs to the solvent. By calculating the overall relaxation time to the solvent as the time that energy takes to decrease in a factor $1/e$ of its initial value, we obtain the values of 9.0 ps and 8.6 ps for the acetyl and amino-end amide I modes, respectively. The transfer of energy into the solvent depends, therefore, only slightly on initial excitation of the acetyl-end or the amino-end amide I mode.

We have used the SMF method to investigate which INMs transfer more energy into the solvent, apart from the amide I mode. The results are shown in Figure 5. We notice in this figure that the amounts of energy transferred from the initially excited acetyl and amino-end amide I modes, 238.0 cm^{-1} and 171.5 cm^{-1} which correspond to 14.0% and 9.6% of the initial excitation energy of the amide I modes, respectively, are out of the scale. As observed, the amount of energy transferred into the solvent tends to be larger as the frequency of the INM decreases. To guide the eye, we include in the figure the dashed lines corresponding to the average energies transferred to the solvent by all the INMs, which are $1638.3/60 \simeq 27.3$ cm^{-1} and $1685.7/60 \simeq 28.1$ cm^{-1} for the acetyl-end and the amino-end amide I modes, respectively. The contributions of the lower frequency INMs are all above the average energy, while the contributions of the higher frequency modes are always below that energy. This is the same behavior as observed in the relaxation of the amide I mode of NMAD,[72] where low frequency modes act as doorways for the intermolecular energy flow into the solvent. There are some few mid-frequency modes deviating from the general trend which transfer significant amounts of energy to the

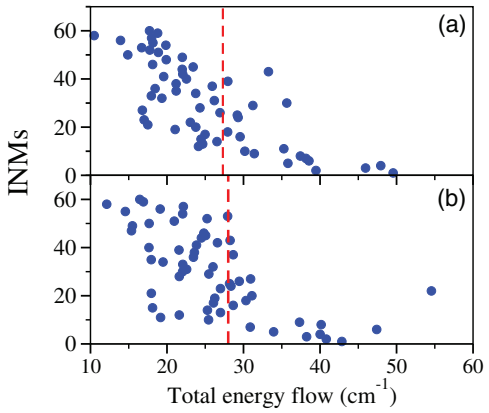

FIG. 5. Vibrational energy (in cm^{-1}) transferred from the INMs of the ^{13}C-AlaD-d_2 molecule into the D_2O solvent after initial excitation of the (a) acetyl and (b) amino-end amide I modes, as calculated using the SMF method. INMs are labeled as in Table V. Dashed lines indicate the average energy transfer per mode.

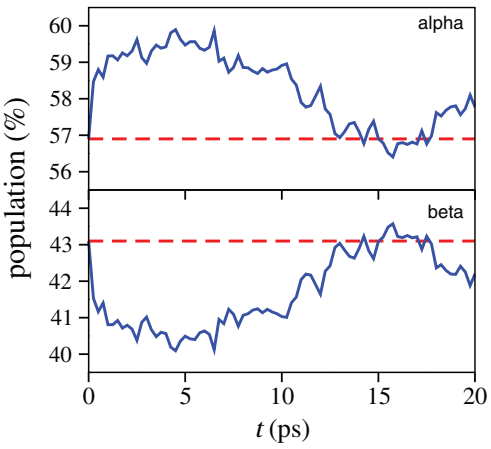

FIG. 6. Conformational populations (in %) as a function of time (averaged over 0.25 ps intervals) of the AlaD-d_2 molecule in liquid D_2O obtained from nonequilibrium MD simulations when the acetyl-end amide I was initially excited (blue lines) and the corresponding equilibrium values (dashed red lines).

solvent, such as the 30th INMs in the relaxation of the acetyl-end amide I mode, and the 22nd INM in the relaxation of the amino-end mode. As discussed above, these INMs are highly excited during the relaxation IVR process.

4. Time evolution of the conformer populations

Let us finally consider the time evolution of the populations of the alpha and beta conformer regions of the AlaD molecule during the relaxation process. To facilitate comparison with previous conformational studies[21,29] we have analyzed in detail the dynamics of the ^{12}C AlaD-d_2 molecule in D_2O, and also performed some tests for the ^{13}C AlaD-d_2 molecule that show that conformer populations are largely unaffected by that isotopic ^{12}C/^{13}C substitution. We have first evaluated the average populations of the alpha/beta conformers extracted from equilibrium MD simulations. From two independent simulation sets, we have thus obtained populations of 56.9% and 43.1%, respectively, for the alpha and beta regions of the AlaD-d_2/$D_2O_{(l)}$ system, and populations of 56.6% and 43.4% for the alpha and beta regions of the AlaD/$H_2O_{(l)}$ system. These results indicate that the H/D isotopic substitution does not have an appreciable effect in the conformer populations either. Previous studies by Feig[21] and by Hu *et al.*[29] provide in addition equal populations for both conformers for the AlaD/$H_2O_{(l)}$ system, somewhat in contrast with our results slightly favoring the alpha region conformers. This difference is probably due to the use of the NVE ensemble in our simulations, versus the NPT and NVT ensembles employed in Refs. 29 and 21, respectively.

Figure 6 shows the time evolution of the populations of the alpha/beta region conformers during relaxation of the AlaD-d_2 molecule in D_2O after excitation of the acetyl-end amide I mode. To smooth the curve, we plot values averaged at time intervals of every 0.25 ps. As observed, the population of the alpha region conformers increases during the first 5 ps until reaching a percentage of 60%, with the consequent decrease of the population of the beta region conformers. Interestingly, this partial alpha-to-beta conformers conversion occurs in a time scale similar to that required by the AlaD-d_2 molecule to redistribute its excess energy through IVR. At longer times, the system undergoes the reverse beta-to-alpha conformers conversion, recovering the initial equilibrium populations being after 15 ps. While the changes of conformer populations shown in Figure 6 are modest, they are in our view an excellent example of how small amounts of vibrational energy can alter the conformation of peptides.

IV. CONCLUSIONS

In this paper we have carried out nonequilibrium Molecular Dynamics simulations of the vibrational relaxation of the amide I modes of the alanine dipeptide molecule dissolved in water, and used the INMs based methodology to analyze the energy flow within the molecule. The identities of the INMs are tracked by using the ENMs as templates. A new definition of the overlap matrix between both sets of normal modes is introduced which allows us to apply the INM based method directly using the output of standard MD packages in terms of space-fixed atomic Cartesian coordinates. The resulting Effective Atomic Min Cost algorithm can also be used to describe flexible molecules such as polypeptides. By using the AlaD molecule as a test case it has been shown that the identification of the INMs does not depend on the set of ENMs chosen as templates, which facilitates the application of the EAMC algorithm to larger molecules with multiple equilibrium configurations.

We have tested different Molecular Mechanics force fields to describe the AlaD molecule, concluding that the CHARMM22 force field is the best since it localizes every amide I mode on each carbonyl group, in agreement with the experimental findings, while the AMBER94 and OPLS-AA/L force fields lead to amide I modes delocalized over both CO groups.

The MD energy relaxations of the acetyl and amino-end amide I modes exhibit a biexponential decay and are in good agreement with the measured data. Using the Statistical

Minimum Flow method, we have identified the different intra- and intermolecular relaxation pathways of the amide I modes. Most of the vibrational energy deposited in these modes is released through IVR exciting many intermediate INMs under frequency resonance conditions. The amount of energy that flows into the solvent grows as the frequency of the INM decreases, and the rate at which the energy is transferred is similar after initial excitation of any of the acetyl-end or amino-end amide I mode.

The relaxation process also alters the equilibrium populations of the alpha and beta region conformers of the AlaD molecule. During the first 5 ps, which corresponds roughly to the time required by the AlaD molecule to redistribute its excess energy through IVR, the population of the alpha region conformers increases—and that of the beta region conformers consequently decreases—and the equilibrium populations are recovered after 15 ps.

ACKNOWLEDGMENTS

This work was partially supported by the Ministerio de Ciencia e Innovación of Spain under Projects CTQ2011-25872 and CONSOLIDER CSD2009-00038, and by the Fundación Séneca del Centro de Coordinación de la Investigación de la Región de Murcia under Project 08735/PI/08. M.H.F. gratefully acknowledges a fellowship from the Ministerio de Ciencia e Innovación of Spain.

[1]D. M. Leitner, Annu. Rev. Phys. Chem. **59**, 233 (2008).
[2]D. M. Leitner and J. E. Straub, *Proteins: Energy, Heat and Signal Flow (Computation in Chemistry)* (Taylor and Francis Group, Boca Raton, 2010).
[3]H. Fujisaki and J. E. Straub, J. Phys. Chem. B **111**, 12017 (2007).
[4]H. Fujisaki, Y. Zhang, and J. Straub, *Advancing Theory for Kinetics and Dynamics of Complex, Many-Dimensional Systems: Clusters and Proteins*, Advances in Chemical Physics Vol. 145, edited by T. Komatsuzaki, R. S. Berry, and D. M. Leitner, (Wiley-Blackwell, 2011), pp. 1–33.
[5]R. J. D. Miller, Annu. Rev. Phys. Chem. **42**, 581 (1991).
[6]Y. Mizutani and T. Kitagawa, Science **278**, 443 (1997).
[7]P. Hamm, M. H. Lim, and R. M. Hochstrasser, J. Phys. Chem. B **102**, 6123 (1998).
[8]D. D. Dlott, Chem. Phys. **266**, 149 (2001).
[9]S. Mukamel and R. M. Hochstrasser, Chem. Phys. **266**, 135 (2001).
[10]M. T. Zanni, M. C. Asplund, and R. M. Hochstrasser, J. Chem. Phys. **114**, 4579 (2001).
[11]M. D. Fayer, Annu. Rev. Phys. Chem. **52**, 315 (2001).
[12]S. Woutersen and P. Hamm, J. Phys.: Condens. Matter **14**, R1035 (2002).
[13]A. M. Nagy, V. I. Prokhorenko, and R. J. D. Miller, Curr. Opin. Struct. Biol. **16**, 654 (2006).
[14]L. P. DeFlores, Z. Ganim, S. F. Ackley, H. S. Chung, and A. Tokmakoff, J. Phys. Chem. B **110**, 18973 (2006).
[15]Z. Wang, J. A. Carter, A. Lagutchev, Y. K. Koh, N.-H. Seong, D. G. Cahill, and D. D. Dlott, Science **317**, 787 (2007).
[16]P. Hamm, J. Helbing, and J. Bredenbeck, Annu. Rev. Phys. Chem. **59**, 291 (2008).
[17]M. D. Fayer, Annu. Rev. Phys. Chem. **60**, 21 (2009).
[18]M. Feig, J. Chem. Theory Comput. **3**, 1734 (2007).
[19]P. Nguyen, S. Park, and G. Stock, J. Chem. Phys. **132**, 025102 (2010).
[20]M. Kobus, P. Nguyen, and G. Stock, J. Chem. Phys. **134**, 124518 (2011).
[21]M. Feig, J. Chem. Theory Comput. **4**, 1555 (2008).
[22]J. T. Edsall, P. J. Flory, J. C. Kenndrew, and A. M. Liquori, Biopolymers **4**, 121 (1966).
[23]T. Head-Gordon, M. Head-Gordon, M. J. Frisch, C. L. Brooks, and J. A. Pople, J. Am. Chem. Soc. **113**, 5989 (1991).
[24]R. I. Gould and P. A. Kollman, J. Phys. Chem. **96**, 9255 (1992).
[25]L. Schafer, I. S. Bindrees, R. F. Frey, C. Vanalsenoy, and C. Ewbank, J. Mol. Struct.: THEOCHEM **338**, 71 (1995).
[26]W. G. Han, K. J. Jalkanen, M. Elstner, and S. Suhai, J. Phys. Chem. B **102**, 2587 (1998).
[27]P. E. Smith, J. Chem. Phys. **111**, 5568 (1999).
[28]S. Gnanakaran and R. M. Hochstrasser, J. Am. Chem. Soc. **123**, 12886 (2001).
[29]H. Hu, M. Elstner, and J. Hermans, Proteins **50**, 451 (2003).
[30]A. N. Drozdov, A. Grossfield, and R. V. Pappu, J. Am. Chem. Soc. **126**, 2574 (2004).
[31]D. S. Chekmarev, T. Ishida, and R. M. Levy, J. Phys. Chem. B **108**, 19487 (2004).
[32]Z.-X. Wang and Y. Duan, J. Comput. Chem. **25**, 1699 (2004).
[33]Y. S. Kim, J. Wang, and R. M. Hochstrasser, J. Phys. Chem. B **109**, 7511 (2005).
[34]G. Seabra, R. C. Walker, E. M. Elstner, D. A. Case, and A. E. Roitberg, J. Phys. Chem. A **111**, 5655 (2007).
[35]K. Kwac, K.-K. Lee, J. B. Han, K.-I. Oh, and M. Cho, J. Chem. Phys. **128**, 105106 (2008).
[36]S. Yang and M. Cho, J. Chem. Phys. **131**, 135102 (2009).
[37]M. P. Gaigeot, Phys. Chem. Chem. Phys. **12**, 10198 (2010).
[38]C.-D. Poon, E. T. Samulski, C. F. Weise, and J. C. Weisshaar, J. Am. Chem. Soc. **122**, 5642 (2000).
[39]C. F. Weise and J. C. Weisshaar, J. Phys. Chem. B **107**, 3265 (2003).
[40]T. Takekiyo, T. Imai, M. Kato, and Y. Taniguchi, Biopolymers **173**, 283 (2004).
[41]M. A. Mehta, E. A. Fry, M. T. Eddy, M. T. Dedeo, A. E. Anagnost, and J. R. Long, J. Phys. Chem. B **108**, 2777 (2004).
[42]Y. S. Kim and R. M. Hochstrasser, J. Phys. Chem. B **109**, 6884 (2005).
[43]K.-K. Lee, K.-I. Oh, H. Lee, C. Joo, H. Han, and M. Cho, ChemPhysChem **8**, 2218 (2007).
[44]J. Grdadolnik, S. G. Grdadolnik, and F. Avbelj, J. Phys. Chem. B **112**, 2712 (2008).
[45]A. Bastida, M. A. Soler, J. Zuñiga, A. Requena, A. Kalstein, and S. Fernandez-Alberti, J. Chem. Phys. **132**, 224501 (2010).
[46]A. Bastida, M. A. Soler, J. Zuñiga, A. Requena, A. Kalstein, and S. Fernandez-Alberti, J. Phys. Chem. A **114**, 11450 (2010).
[47]A. Kalstein, S. Fernández-Alberti, A. Bastida, M. A. Soler, M. H. Farag, J. Zuñiga, and A. Requena, Theor. Chem. Acc. **128**, 769 (2011).
[48]A. Bastida, M. A. Soler, J. Zuñiga, A. Requena, A. Kalstein, and S. Fernandez-Alberti, J. Phys. Chem. B **116**, 2969 (2012).
[49]Y. Fang, S. Shigeto, N. Seong, and D. Dlott, J. Phys. Chem. A **113**, 75 (2009).
[50]P. Ren and J. Ponder, J. Comput. Chem. **23**, 1497 (2002).
[51]P. Ren and J. Ponder, J. Phys. Chem. B **107**, 5933 (2003).
[52]A. D. MacKerell, D. Bashford, M. Bellott, R. L. Dunbrack, J. D. Evanseck, M. J. Field, S. Fischer, J. Gao, H. Guo, S. Ha, D. Joseph-McCarthy, L. Kuchnir, K. Kuczera, F. T. K. Lau, C. Mattos, S. Michnick, T. Ngo, D. T. Nguyen, B. Prodhom, W. E. Reiher, B. Roux, M. Schlenkrich, J. C. Smith, R. Stote, J. Straub, M. Watanabe, J. Wiórkiewicz-Kuczera, D. Yin, and M. Karplus, J. Phys. Chem. B **102**, 3586 (1998).
[53]W. D. Cornell, P. Cieplak, C. I. Bayly, I. R. Gould, J. K. M. Merz, D. M. Ferguson, D. C. Spellmeyer, T. Fox, J. W. Caldwell, and P. A. Kollman, J. Am. Chem. Soc. **117**, 5179 (1995).
[54]W. L. Jorgensen, D. S. Maxwell, and J. Tirado-Rives, J. Am. Chem. Soc. **118**, 11225 (1996).
[55]G. A. Kaminski, R. A. Friesner, J. Tirado-Rives, and W. L. Jorgensen, J. Phys. Chem. B **105**, 6474 (2001).
[56]H. J. C. Berendsen, J. P. M. Postma, W. F. van Gunsteren, A. DiNola, and J. R. Haak, J. Chem. Phys. **81**, 3684 (1984).
[57]A. Balázs, J. Phys. Chem. **94**, 2754 (1990).
[58]H. J. Boehm and S. Brode, J. Am. Chem. Soc. **113**, 7129 (1991).
[59]I. R. Gould, W. D. Cornell, and I. H. Hillier, J. Am. Chem. Soc. **116**, 9250 (1994).
[60]D. M. Philipp and R. A. Friesner, J. Comput. Chem. **20**, 1468 (1999).
[61]R. Vargas, J. Garza, B. P. Hay, and D. A. Dixon, J. Phys. Chem. A **106**, 3213 (2002).
[62]C. Chipot and A. Pohorille, J. Phys. Chem. B **102**, 281 (1998).
[63]M. Lee, S. Y. Lee, S.-W. Joo, and K.-H. Cho, J. Phys. Chem. B **113**, 6894 (2009).
[64]H. Torii, T. Tatsumi, and M. Tasumi, J. Raman Spectrosc. **29**, 537 (1998).
[65]S. Ham, J.-H. Kim, H. Lee, and M. Cho, J. Chem. Phys. **118**, 3491 (2003).
[66]S. Ham and M. Cho, J. Chem. Phys. **118**, 6915 (2003).

[67]K. Moritsugu, O. Miyashita, and A. Kidera, Phys. Rev. Lett. **85**, 3970 (2000).
[68]K. Moritsugu, O. Miyashita, and A. Kidera, J. Phys. Chem. B **107**, 3309 (2003).
[69]Y. Grenie, M. Avignon, and C. Garrigou-Lagrange, J. Mol. Struct. **24**, 293 (1975).
[70]G. Pohl, A. Perczel, E. Vass, G. Magyarfalvi, and G. Tarczay, Phys. Chem. Chem. Phys. **9**, 4698 (2007).
[71]See supplementary material at http://dx.doi.org/10.1063/1.4805086 for additional tables and figures.
[72]M. Soler, A. Bastida, M. H. Farag, J. Zuñiga, and A. Requena, J. Chem. Phys. **135**, 204106 (2011).
[73]J. Max and C. Chapados, J. Chem. Phys. **131**, 184505 (2009).
[74]I. Ohmine and H. Tanaka, J. Chem. Phys. **93**, 8138 (1990).
[75]H. Fujisaki, K. Yagi, J. E. Straub, and G. Stock, Int. J. Quantum Chem. **109**, 2047 (2009).